THE ASTROPHYSICAL JOURNAL, 356:87–99, 1990 June 10


# WEAKLY BARRED EARLY-TYPE RINGED GALAXIES. III. THE REMARKABLE OUTER-RINGED S0$^+$ GALAXY NGC 7020

R. BUTA
Department of Physics and Astronomy, University of Alabama
*Received 1989 August 28; accepted 1989 December 12*

## ABSTRACT

The southern S0$^+$ galaxy NGC 7020 presents an unusual morphology: it includes a very regular outer ring which is completely detached and which envelops an inner ring/lens zone with an exotic *hexagonal* shape. The ring has a high contrast compared with those usually observed in barred galaxies, yet NGC 7020 is not obviously barred. In this paper the structure of this galaxy is studied by means of *UBVRI* CCD surface photometry. The photometry reveals a complex system and shows that most of the recent star formation in the galaxy has taken place in the outer ring. Two bright knots are found on the major axis of the hexagonal zone that appear to be true enhancements of old stars rather than young associations. Between these knots and the bulge there are dips in the surface brightness and a clear zone of *rectangular* isophotes. The combination of these rectangular isophotes and the hexagonal ones gives the impression of an "X"-shaped structure in the inner regions that bears a strong resemblance to what has been seen in the edge-on galaxy IC 4767 studied by Whitmore and Bell. This resemblance is interesting because of the suggestion by Whitmore and Bell that "X" structures could be due to accretion of matter associated with a merger or tidal encounter between an S0 and a small satellite galaxy. Except for the X, there is no clear evidence for such an encounter in the present appearance of NGC 7020, although it is a member of a sparse group. The presence of the outer ring and the non–edge-on orientation of the galaxy suggests the alternative interpretation that the hexagonal/X zone is related to an unusual type of bar or bisymmetric distortion where 4:1 and/or 6:1 resonant orbits are important in influencing the morphology. Both interpretations have difficulties which could probably be resolved with kinematic observations.

*Subject headings:* galaxies: individual (NGC 7020) — galaxies: photometry — galaxies: structure

## I. INTRODUCTION

The nature of outer rings in disk galaxies is only beginning to be explored. The best known of such structures generally appear in barred galaxies and are mostly separated from the inner regions; NGC 1291 (de Vaucouleurs 1975), NGC 2859 (Sandage 1961), and NGC 3945 (Kormendy 1979) are especially good examples. In the *Reference Catalogue of Bright Galaxies* (RC1; de Vaucouleurs and de Vaucouleurs 1964), only about 4% of the galaxies have an outer ring structure, but most interesting is the prevalence of these rings near the stage S0/a (de Vaucouleurs 1975). The origin of outer rings has been discussed by Gallagher and Wirth (1980) and Kormendy (1982), who, on the basis of photoelectric measures of ring colors and the morphological work of Kormendy (1979), suggested that these features owe their existence to the influence of bars or oval distortions which drive repeated episodes of star formation or which rearrange disk material over long-term secular evolution. Schwarz (1981) studied the role of resonances on these processes; his simulations showed how bars can rearrange gas into rings near resonances, and in particular he suggested that outer rings are linked to the outer Lindblad resonance (OLR), where gas is gathered into 2:1 resonant orbits outside corotation (CR). This prediction was tested and confirmed to some extent by statistical studies (Athanassoula *et al.* 1982; Buta 1984, 1986), and for most outer rings Schwarz's explanation is probably correct. Both a bar and an adequate amount of gas near or beyond the resonance seem to be the main requirements. However, there exist striking outer-ringed galaxies which appear to possess little or no obvious bar. One of the best-known cases, Hoag's object (Brosch 1985; Schweizer *et al.* 1987) has a perfect circular, completely detached outer ring and no trace whatsoever of a bar. Such galaxies are very difficult to understand in the context of orbit resonance theory, and indeed Schweizer *et al.* (1987) believe that the ring of Hoag's object is an *accretion* feature, like a polar ring.

In this third paper of the series, I present photometric data on NGC 7020, one of the largest and nearest examples of an apparently nonbarred, outer-ringed galaxy in the sky. It is an S0$^+$ system whose morphology is dominated by a detached outer ring of high contrast. Inside this ring one does not really find a bar, but instead there is an exotic inner ring/lens region whose outer edge appears distinctly *hexagonal* and whose major axis contains two bright knots. Such an unusual structure is rare and not well understood. With *UBVRI* CCD surface photometry, the structure of NGC 7020 is explored and compared with the structure of ringed *barred* galaxies and the previous two objects, NGC 3081 (Buta 1990*a*, hereafter Paper I) and NGC 7187 (Buta 1990*b*, hereafter Paper II). The observations are described in § II, while § III describes the morphology. An analysis of the data is presented in § IV, with a discussion in § V. Conclusions are presented in § VI.

## II. OBSERVATIONS

The observations were made with the 3.9 m Anglo-Australian telescope on 1984 October 24 UT with the RGO CCD camera and an RCA SID 53612 chip having 320 × 512 pixels, each 0″.49 × 0″.49 in size. Filters chosen to match the Johnson *UBV* and Cousins *RI* systems were used. The galaxy was too large for the field of view (2′.6 × 4′.2), so the following

TABLE 1

OBSERVING LOG OF CCD IMAGES

| Filter | Sky[a] (ADU) | Exposure (s) | $\mu_s$(Ap)[b] (mag arcsec$^{-2}$) | $\mu_s$(S.S.)[c] (mag arcsec$^{-2}$) | Seeing[d] ($\sigma_1^*$) | Image Location |
|---|---|---|---|---|---|---|
| $U$...... | 155 | 1000 | 21.19 | 21.15 | 0.77 | Central |
| $B$...... | 135 | 300 | 22.16 | 22.11 | 0.82 | Central |
| $B$...... | 96 | 225 | 22.24 | 22.18 | 0.74 | Central |
| $V$....... | 215 | 225 | 21.29 | 21.24 | 0.77 | Central |
| $R$...... | 195 | 150 | 20.73 | 20.69 | 0.71 | Central |
| $I$....... | 776 | 200 | 19.16 | 19.11 | 0.72 | Central |
| $I$....... | 277 | 72 | 19.19 | 19.13 | 0.72 | Central |
| $V$...... | 230 | 225 | 21.19 | 21.15 | 0.94 | 1'.3 N |
| $V$....... | 230 | 225 | 21.19 | 21.15 | 0.90 | 1'.3 S |
| $R$...... | 195 | 150 | 20.70 | 20.67 | 0.82 | 1'.3 N |
| $R$...... | 195 | 150 | 20.70 | 20.67 | 0.69 | 1'.3 S |
| $I$....... | 773 | 200 | 19.14 | 19.11 | 0.82 | 1'.3 N |
| $I$....... | 773 | 200 | 19.14 | 19.11 | 0.89 | 1'.3 S |

[a] ADU = analog to digital units.
[b] Based on aperture photometry.
[c] Based on CCD standard stars.
[d] Half-width of inner Gaussian component (arcsec).

procedure was used. A central image was obtained in each filter with the long axis of the CCD aligned along the minor axis of the galaxy (≈east-west). Then, for $V$, $R$, and $I$ only, two additional fields offset 1'.3 north and 1'.3 south were obtained to allow construction of a mosaic. The overlap between the central images and the offset images was used to match the coordinate systems of the offset images, which were found to miss overlapping each other by only about 1.5 pixels. The blank zone between them was simply interpolated. A total of seven central images was obtained, and three mosaics. On all images the orientation of the CCD along the galaxy minor axis left only a barely adequate amount of sky. Standard reduction techniques were applied as described in Paper I.

Table 1 lists the details of the images. Zero points and transformation equations were calculated from standard stars for all five filters, but for each filter an independent zero point could be obtained from photoelectric aperture photometry. This photometry was mostly taken from Longo and de Vaucouleurs (1983, 1985) and from Lauberts and Sadler (1984). In addition, a few observations were obtained on 1984 May 25 and June 2 with an EMI 9659 photometer on the 1.0 m and 0.6 m telescopes of the Siding Spring Observatory (Table 2). Table 1 compares the zero points determined from both methods. The agreement is good, but it was found that the part of the night when the CCD observations were made was not completely photometric, so that the standard star zero points should be less reliable than the aperture photometry zero points. Final calibration therefore used the transformation slopes from the standards and zero points from the aperture photometry.

TABLE 2

APERTURE PHOTOMETRY OF NGC 7020

| log $A$[a] | $V$ | $B-V$ | $U-B$ | $V-R$ | $R-I$ | Telescope |
|---|---|---|---|---|---|---|
| 0.43...... | 13.38 | 1.00 | 0.53 | 0.59 | 0.62 | 0.6 m |
| 0.81...... | 12.71 | 1.01 | 0.53 | 0.57 | 0.64 | 0.6 m |
| 1.12...... | 12.27 | 0.98 | 0.45 | 0.54 | 0.64 | 0.6 m |
| 1.19...... | 12.16 | 1.01 | 0.53 | ... | ... | 1.0 m |
| 1.42...... | 11.98 | 0.92 | 0.52 | 0.51: | 0.44: | 0.6 m |

[a] Aperture A in units of 0'.1.

The large amount of aperture photometry proved useful not only for evaluating zero points but also for revealing systematic errors in the surface photometry. Figure 1 shows simulated color-aperture relations compared with the photoelectric measurements. These are based on the central images only using the shortest exposure $B$ and $I$-band images. Although for

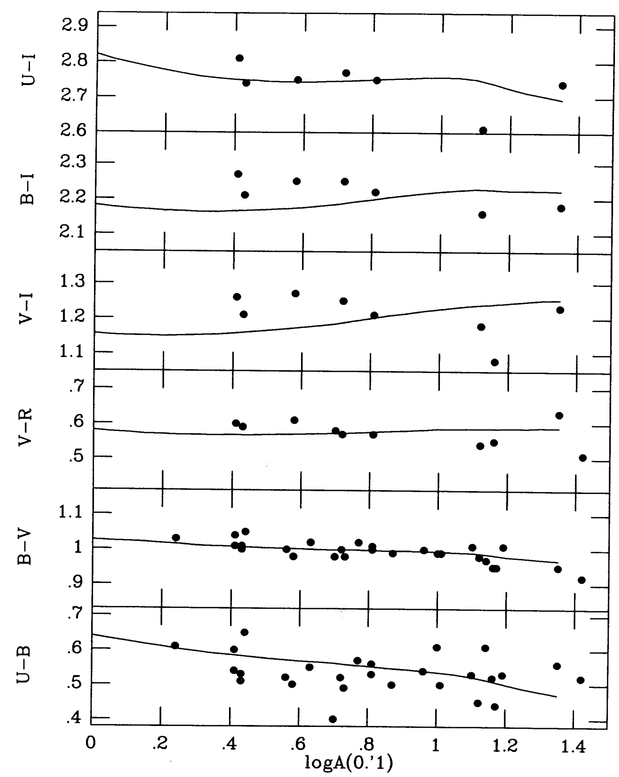


FIG. 1.—Color-aperture relations for NGC 7020. Solid curves are simulated from the surface photometry and take into account zero-point and transformation relations based on standard stars and aperture photometry. Filled circles are available photoelectric measurements for comparison. Departures of the curves from these data show that systematic errors are present in the $I$-band surface brightnesses.

$U-B$ and $B-V$ the agreement between the simulated relations and the extensive aperture photometry seems good, the relations involving the $I$-band (and to a lesser extent the $R$ band) do not agree with the observed relations. No clear-cut cause for the disagreements was found, although a nonlinearity of the CCD is the probable explanation. Color index maps revealed that the problem is manifested mostly along the minor-axis direction of the galaxy, where the intensity gradient is steepest. This makes the present surface photometry, at least in the redder colors, less precise than would be desired, but it is still useful for structural studies, particularly in the intermediate ranges of surface brightness.

## III. MORPHOLOGY AND GROUP MEMBERSHIP

Figure 2*a* (Plate 1) shows the mosaic $V$-band image of NGC 7020. Two distinct zones are evident. The most prominent zone is the outer ring, 2′.6 in diameter and completely detached from the inner regions. The ring is broad and mildly feathery in blue light, and appears to have a fairly uniform surface brightness in azimuth. Inside the ring and separated from it by a wide gap, an inner lenslike zone is evident. In the *Second Reference Catalogue of Bright Galaxies* (RC2; de Vaucouleurs, de Vaucouleurs, and Corwin 1976), this inner zone is recognized as an inner ring.

The inner zone shows other interesting features which are identified in the enlargement in Figure 2*b* (Plate 2). In particular, at its major axis there are two diffuse, round knots, features which, in S0 galaxies, might be recognized as the edge-on view of an inner ring. However, the shape of the outer ring tells us that NGC 7020 is not edge-on but is tilted only about 70°; this suggests that the knots are not artifacts of tilt but are distinct objects. The edge of the inner lens just outside the knots shows a remarkably regular *hexagonal* shape that is evident in all five filters. This shape is distinguishable even at the scale of the SRC $J$ Sky Survey charts.

In the zone between the nucleus and the knots, there are subtle depressions in the surface brightness whose shape gives the impression that an "X" crosses the nucleus (see arrows in Fig. 2*b*). Such a structure has actually been noted in another galaxy (Whitmore and Bell 1988) and is not well understood. The "X"-shape gives one the impression that the galaxy has two "bars," but it is unclear what such a structure means from the point of view of dynamics if it is real. The "X"-shape is quantified better in § IV*d*, and its dynamical implications are discussed further in § V.

Figure 3 (Plate 3) shows a $B-V$ color index map of NGC 7020. The main feature evident in this map is that the outer ring is a clear blue enhancement compared with the hexagonal zone and the gap region. The two knots show little or no distinct color enhancement compared with their surroundings. It appears that they are old stellar objects and not unusual associations. In a $U-B$ map (not shown) there is a definite patchiness in the outer ring which suggests the presence of faint associations. *Thus most of the recent star formation in NGC 7020 has taken place in the outer ring.*

NGC 7020 is an original Shapley-Ames (1932) galaxy and consequently is included in many catalogs. Table 3 summarizes type estimates from three catalogs: the ESO $B$ Catalog (Lauberts 1982), the *Southern Galaxy Catalogue* (SGC; Corwin, de Vaucouleurs, and de Vaucouleurs 1985), and the *Revised Shapley-Ames Catalog* (RSA; Sandage and Tammann 1981). RC2 gives a type estimate of (R)SA(r)0$^+$ made by de Vaucouleurs (1963) based on a Boyden 60 inch (1.5 m) reflector plate, but interestingly de Vaucouleurs's first type estimate based on a Reynolds reflector plate is (R)SAB0 [or (R)SA0$^+$?; de Vaucouleurs 1956]. The different sources are in agreement that the galaxy is a late S0, but the family seems uncertain. My adopted type in Table 3 is based on considerations discussed in § V.

The group membership of NGC 7020 was assessed using data in the *Third Reference Catalogue of Bright Galaxies* (RC3, de Vaucouleurs *et al.* 1989). In RC3 there are five entries within 1° of NGC 7020, three of which have a measured redshift. The mean redshift of these three (IC 5084, IC 5092, and IC 5096) is

TABLE 3

BASIC AND INTEGRATED PARAMETERS[a]

| Parameter | Value | Parameter | Value |
|---|---|---|---|
| $\alpha$ | $21^h07^m13^s$ | $\log D_{25}$ | 1.536 |
| $\delta$ | $-64°13'48''$ | $\log R_{25}$ | 0.345 |
| $l$ | 330°.6 | $\theta_{25}$ | 165° |
| $b$ | −39°.3 | $C_{21}(V)$ | 2.65 |
| SGL | 220°.4 | $C_{32}(V)$ | 2.24 |
| SGB | 6°.1 | $r_1^*(V)$ | 0′.144 |
| ESO $B$ type | SB0 | $r_e^*(V)$ | 0′.382 |
| SGC type | (R)SA(r)0$^+$: pec | $r_3^*(V)$ | 0′.856 |
| RSA type | RS0$_2$/RSa | $\mu_1(V)$ | 20.36 mag arcsec$^{-2}$ |
| Adopted type | (R)SAB?(rl)0$^+$ | $\mu_e(V)$ | 21.82 mag arcsec$^{-2}$ |
| $V_T$ | $11.82 \pm 0.03$ | $\mu_3(V)$ | 23.27 mag arcsec$^{-2}$ |
| $\log A_e(B)$ | 0.96 | $m'_e(B)$ | 13.07 mag arcminute$^{-2}$ |
| $(B-V)_T$ | 0.96 | $(B-V)_e$ | 0.99 |
| $(U-B)_T$ | 0.45 | $(U-B)_e$ | 0.54 |
| $(V-R)_T$ | $0.56 \pm 0.03$ | $(V-R)_e$ | $0.57 \pm 0.02$ |
| $q$(d) | $0.437 \pm 0.003$ | $\theta$(d) | 164°.8 ± 0°.2 |
| $i$ | 69° ± 2° | $C_{21}(B)$ | 2.66 |
| $d$(R) | 2′.57 | $\mu_1(B)$ | 21.42 mag arcsec$^{-2}$ |
| $q$(R) | 0.489 | $\mu_e(B)$ | 22.92 mag arcsec$^{-2}$ |
| $\theta$(R) | 162°.4 | $\log D_e(B)$ | 1.119 |
| $r$(knots) | ±34″ | $\log R_e(B)$ | 0.423 |
| $\theta$(knots) | 167°.5 | $\theta_e(B)$ | 166°.7 |

[a] Positional information from ESO $B$ catalog and RC3. $A_e$, $D_{25}$, and $D_e$ are in units of 0′.1.

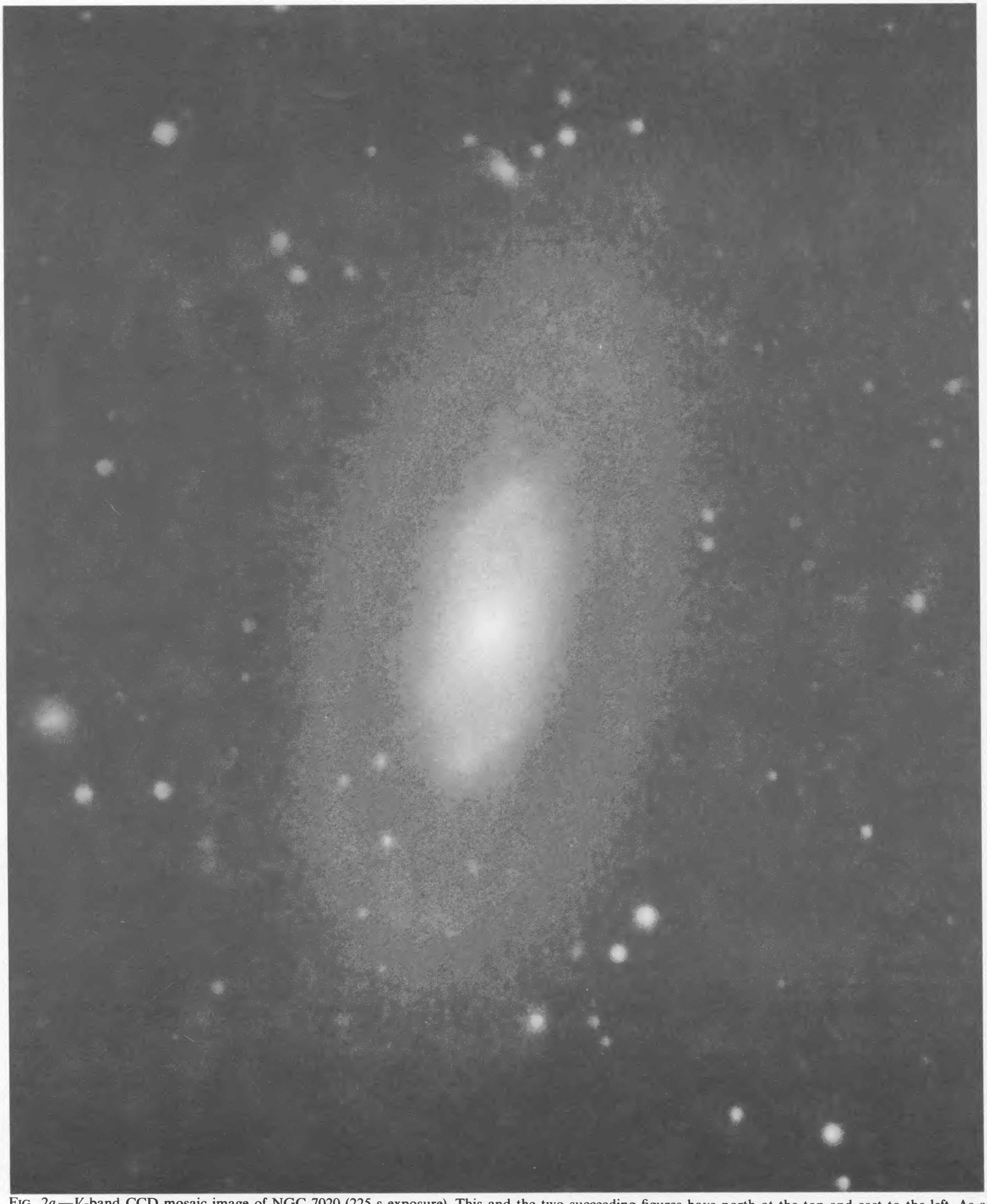

FIG. 2*a*.—*V*-band CCD mosaic image of NGC 7020 (225 s exposure). This and the two succeeding figures have north at the top and east to the left. As an indicator of image scale, the two bright knots at the major-axis points of the inner hexagonal zone are 68″ apart. A bright star lies just outside the field to the north and produces some diffuse light near the top of the image.

BUTA (*see* **356**, 89)

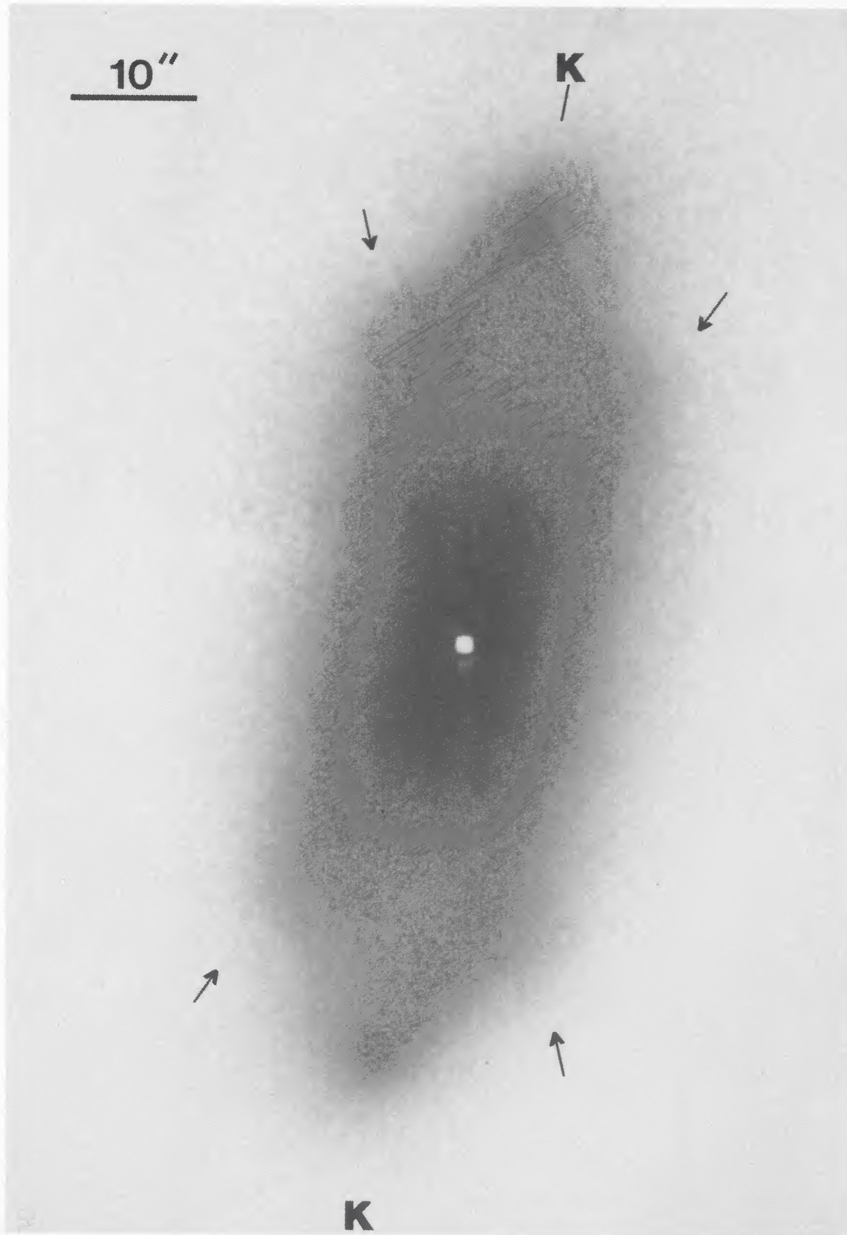


FIG. 2*b*.—Enlargement of the inner zone of NGC 7020. The knots are indicated by the letters "K." Arrows define the position angles of the arms of the "X." This $V$-band image has had the bulge model described in § IV*d* subtracted to enhance the "X." The display is in units of mag arcsec$^{-2}$, and a few faint field stars have been removed.

BUTA (*see* **356**, 89)

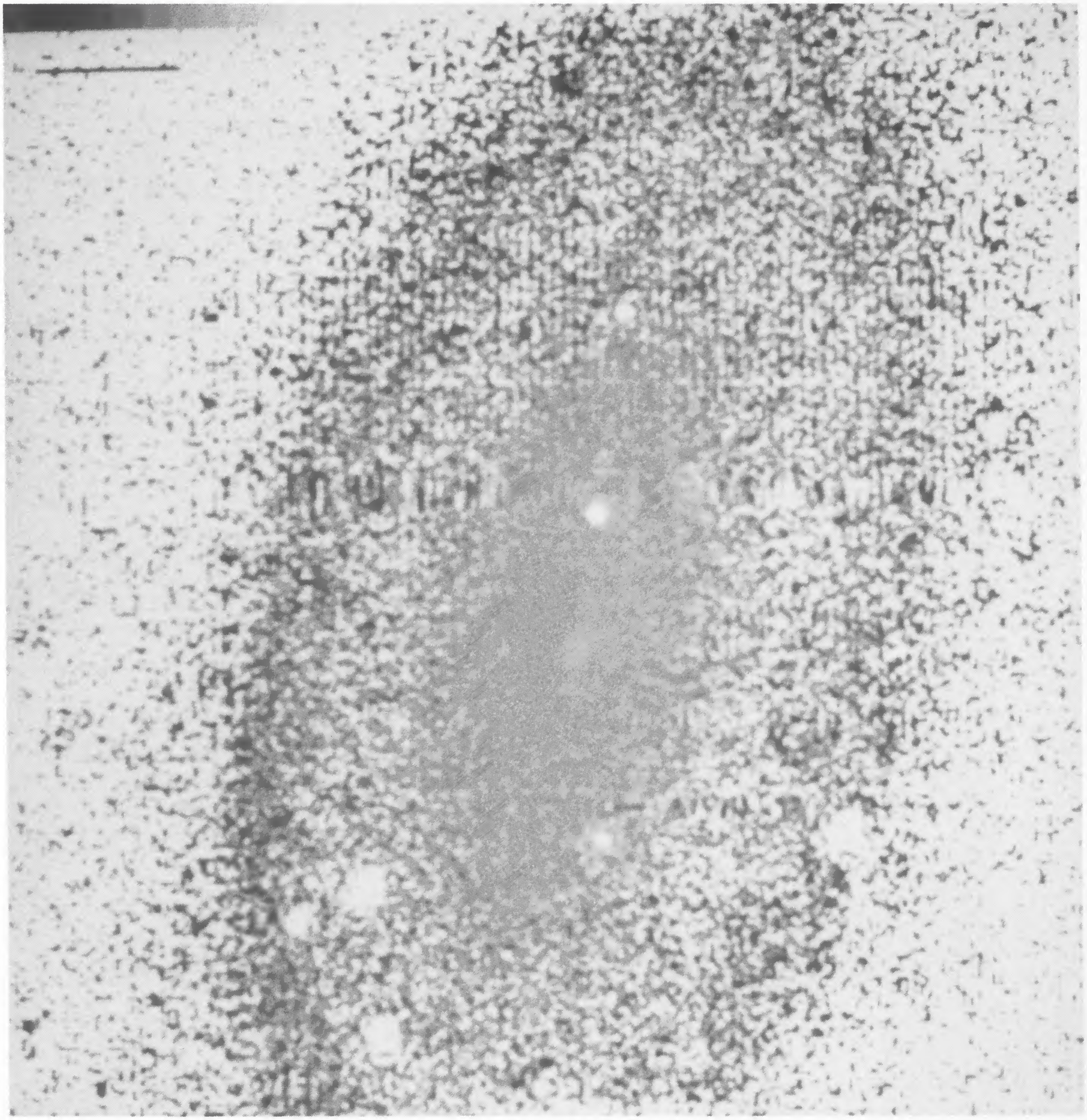

FIG. 3.—$B-V$ color index map of NGC 7020. The dark horizontal bar is 20″ in length. The step scale ranges from $B-V$ = 0.4 (darkest) to 1.4 (lightest) in 0.1 mag steps.

BUTA (*see* **356**, 89)

$\langle V_{\odot} \rangle = 3218$ km s$^{-1}$, which is very close to that for NGC 7020, $V_{\odot} = 2978$ km s$^{-1}$. All three are more than 15 outer ring diameters away from NGC 7020. The closest cataloged object to NGC 7020, ESO 107-14, is 5 outer ring diameters away but has no measured redshift. If we consider galaxies within 3° of NGC 7020, another object, NGC 7083, is found to have a similar redshift, and if we restrict to 6°, five additional objects are found, NGC 6943, ESO 107-4, NGC 7096, NGC 7125, and NGC 7126. Thus NGC 7020 is a member of a sparse grouping or cloud; it in fact lies within region VI of de Vaucouleurs (1956).

NGC 7020 has also been observed by Arp (1981), who measured its redshift (2868 km s$^{-1}$) and also the redshift of a small nearby companion (28,030 km s$^{-1}$). Arp also noted the bright knots along the major axis and commented on some properties of the inner and outer rings.

## IV. DATA ANALYSIS

### a) *Integrated Properties*

The surface photometry was first used to derive a number of basic parameters of NGC 7020 (Table 3). The total magnitude, $V_T = 11.82 \pm 0.03$, was obtained by integrating and extrapolating an elliptically averaged luminosity profile. The $B$-band total magnitude, $B_T$, could not be estimated as directly because no mosaic was obtained in $B$. Instead, $B_T$ could be fairly accurately calculated from $V_T$ and $(B-V)_T$ computed from the integrated $B-V$ color curve in Figure 1. This led to $(B-V)_T = 0.96 \pm 0.02$ and $B_T = 12.78 \pm 0.04$. In the ESO LV data base (Lauberts and Valentijn 1989), the integrated magnitude of NGC 7020 is $B_T(\mathrm{LV}) = 12.81$, in good agreement with my CCD photometry. I also find very good agreement on the integrated $R$-band magnitude: $R_T(\mathrm{CCD}) = 11.22$ versus $R_T(\mathrm{LV}) = 11.27$.

The absolute magnitude of NGC 7020 is calculated using its redshift as an approximate distance indicator. The corrected RC3 velocity reduced to the frame of the nearby galaxies (see Buta and de Vaucouleurs 1983) is $V_c = 2695$ km s$^{-1}$, and using $H_0 = 100$ km s$^{-1}$ Mpc$^{-1}$ gives a distance of 27 Mpc. If $B_T$ is corrected using RC2 procedures, then the absolute magnitude of NGC 7020 is $M_T^0(B) = -20.0$.

Also derived from the surface photometry are the effective aperture, $A_e$, and the diameter of the effective isophote, $D_e$, both of which quantify a size which transmits half of the total $B$-band flux. Standard isophotal parameters $D_{25}$, $R_{25}$, and $\theta_{25}$, which refer to the diameter, axis ratio, and position angle, respectively, of the isophote having $\mu_B = 25.0$ mag arcsec$^{-2}$, were obtained from an ellipse fit. The values for all of these parameters in Table 3 compare favorably with independent estimates in the ESO LV data base.

An equivalent luminosity profile was used to estimate other basic de Vaucouleurs parameters such as the equivalent radii of the "quartiles" of the light distribution (de Vaucouleurs, 1948, 1953, 1977) and the concentration indices $C_{21}$ and $C_{32}$, defined as the ratios of these radii. All three quartile radii could be derived in $V$ light, but in $B$ light only $r_1^*$ and $r_e^*$ could be measured. The concentration indices indicate that NGC 7020 is more concentrated than NGC 3081 or NGC 7187 (Papers I and II).

The integrated colors of NGC 7020 were obtained by extrapolating the profiles in Figure 1. Only $(B-V)_T$, $(U-B)_T$, and $(V-R)_T$ can be regarded as reliable, since colors involving the $I$ band show a systematic error. The corrected colors, $(B-V)_T^0 = 0.80$, $(U-B)_T^0 = 0.34$, are consistent with a late S0 or S0/a system according to de Vaucouleurs (1977).

### b) *Parameters of the Outer Ring and "Knots"*

The apparent size and shape of the outer ring of NGC 7020 were measured using the $V$-band mosaic. A TV display was used to define the ridge line of the feature, and an ellipse was fitted to the ridgeline points. This gave $d(\mathrm{R}) = 2'.57$, $q(\mathrm{R}) = 0.489$, and $\theta(\mathrm{R}) = 162^\circ.4$ for the diameter, axis ratio, and position angle, respectively. The diameter and axis ratio estimates agree well with estimates made by de Vaucouleurs from independent plate material (de Vaucouleurs and Buta 1980*a*). At the distance of 27 Mpc, $1'' = 130$ pc, so the diameter of the outer ring is 20 kpc, larger than the average outer ring according to a preliminary study (Buta 1984).

The positions of the knots of NGC 7020 were estimated using a centroid finding routine. It was found that to within $0''.1$, the two objects are at exactly the same distance from the nucleus, $r = 34''.0 = 4.45$ kpc in the position angle $167^\circ.5$. They are thus very nearly aligned with the projected major axis. The ratio of the outer ring diameter to the separation of the knots, $d(\mathrm{R})/d(\mathrm{K}) = 2.27$, is very close to the mean ratio of outer ring to bar diameters in SB galaxies (Kormendy 1979) and outer to inner ring diameters in double ring SA, SAB, and SB systems (Athanassoula *et al.* 1982; Buta 1984, 1986). The coincidence of this ratio provides support for the interpretation that the hexagonal zone of NGC 7020 is related to an inner ring. On SRC *J* sky survey charts, there is a weak enhancement at the edge of this region. This is the reason for the (rl) interpretation adopted in Table 3, which follows a ring/lens notation used by Kormendy (1979).

### c) *Isophotes and Luminosity Profiles*

Smoothed $V$-band isophotes of NGC 7020 based on the mosaic image are illustrated in Figure 4. These show the symmetric large-scale structure to $\mu_V = 25.0$ mag arcsec$^{-2}$. Higher resolution isophotes of the hexagonal zone are shown in Figure 5. The "X" character weakly visible in the images is not seen in these isophotes, but instead a distinctive sequence of shapes is displayed: the isophotes are nearly circular in the center, then become elliptical, then rectangular, and then hexagonal with increasing radius. The pattern is extremely regular and appears much the same in isophote maps from the other passbands. An important characteristic not readily evident in these plots is that two of the four shorter sides of the hexagonal region are slightly brighter than the other two; in certain contrast settings on a TV monitor, this difference causes the knots to actually appear connected to the northeast and southwest corners of the inner boxy zone via two short spiral arcs (see Fig. 2*b*).

The properties of the isophotes were quantified by fitting ellipses. The dependence of the isophote shapes and orientations on radius is displayed in Figure 6. The minimum axis ratio is achieved near the knots, which are visible in Figure 5. The position angle is nearly constant over most of the disk, but changes by about 20° in the inner 6″. The main parameters derived from these plots are the shape and orientation of the outer disk. To aid further in the derivation of these parameters, I obtained a copy of UK Schmidt Plate J3646 and scanned the field of NGC 7020 with a PDS microdensitometer. A wedge calibration was used to get approximate surface brightnesses, and ellipses were fitted to the region beyond the boxy zone. The results of these fits are plotted as open triangles in Figure

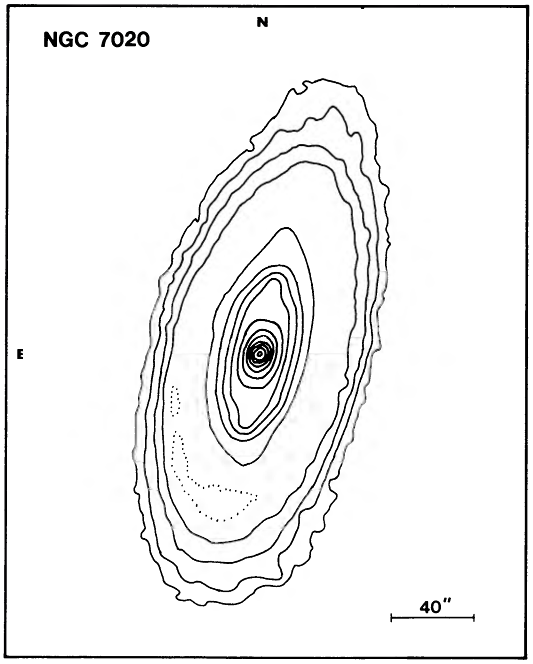


FIG. 4.—$V$-band isophotes of the large-scale structure of NGC 7020. The isophotes were smoothed using a 5".9 × 5".9 box averaging technique. The brightest isophote is at $\mu_V$ = 18.0 mag arcsec$^{-2}$, and each successive isophote is separated by 0.50 mag arcsec$^{-2}$. The dashed isophote is associated with the ridgeline of the outer ring and is at the level $\mu_V$ = 23.0 mag arcsec$^{-2}$.

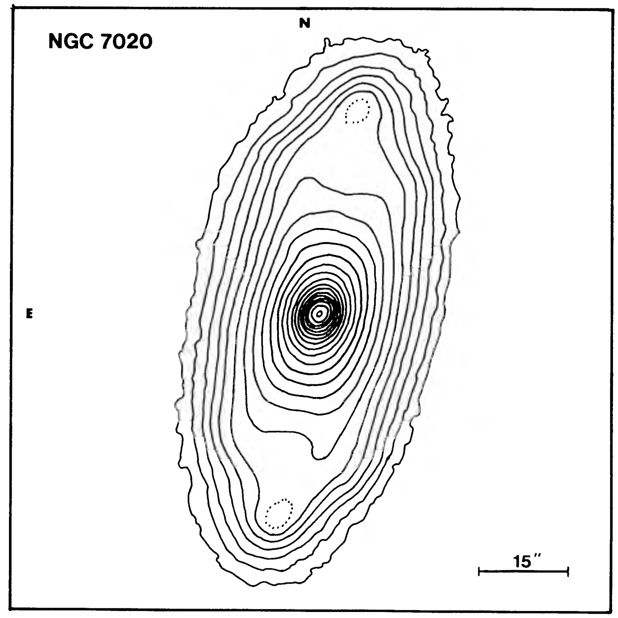


FIG. 5.—$V$-band isophotes of the inner regions of NGC 7020, showing the unusual sequence of isophote shapes. The largest isophote is at $\mu_V$ = 22.75 mag arcsec$^{-2}$, and each successive isophote is separated by −0.25 mag arcsec$^{-2}$, except for the central isophote, which is −0.50 mag arcsec$^{-2}$ brighter than the next one. The isophotes were smoothed using a 0".98 × 0".98 box averaging technique. The small dashed contours are at $\mu_V$ = 21.25 mag arcsec$^{-2}$ and are associated with the two knots shown in Fig. 2*b*.

6. Very good agreement was found for both shape and orientation between the $J$ plate and the CCD mosaic images. The disk shape in the range 110" ≤ $a$ ≤ 132" is ⟨$q$(d)⟩ = 0.437 ± 0.003, and the mean position angle (reduced to epoch 1950) over the same range is ⟨$\theta$(d)⟩ = 164°.8 ± 0°.2. With the adopted shape and using the relation derived by Bottinelli *et al.* (1983) for the type dependence of the intrinsic flattening of the disk, the inclination of NGC 7020 is $i$ = 69° ± 2°, assuming that the disk is intrinsically circular in its plane.

The deviations of the isophotes from ellipses are quantified in Figures 7 and 8. In Figure 7 the Fourier radius amplitudes, $A_m = (a_m^2 + b_m^2)^{1/2}/a$, for $m = 4$ and 6, are shown plotted against radius. Here $a_m$ and $b_m$ are the sine and cosine amplitudes of the radius deviations from a fitted ellipse whose major-axis radius is $a$. These show that significant $m = 4$ and 6 amplitudes (in the range 4%–6%) are present throughout the zone 9" ≤ $a$ ≤ 42". Figure 8 (*bottom panel*) shows the logarithm of the ratio of the amplitudes $A_4/A_6$ versus $a^{1/2}$. The $m = 4$ term appears to be dominant in the range 9" ≤ $a$ ≤ 25" and reaches its maximum amplitude near $a$ = 20". The $m = 6$ term becomes dominant in the range 34" ≤ $a$ ≤ 42" and reaches its maximum amplitude near $a$ = 36". The fits break down in the transition zones between the rectangular and hexagonal isophote zones, and between this latter zone and the outer parts of the outer ring.

Although the $m = 6$ term dominates just outside $a$ = 36", the $m = 4$ term is still significant in the range 36" ≤ $a$ ≤ 52". Figure 8 shows the relative cos 4$\theta$ amplitude $b_4/a$ (*top panel*) and the phase of the 4$\theta$ term, $\theta_4 = \tan^{-1}(a_4/b_4)/4$ (*middle panel*), versus $a^{1/2}$. These parameters are often used to detect boxy isophotes or weak disks in elliptical galaxies (Jedrzejewski, Davies, and Illingworth 1987 and references

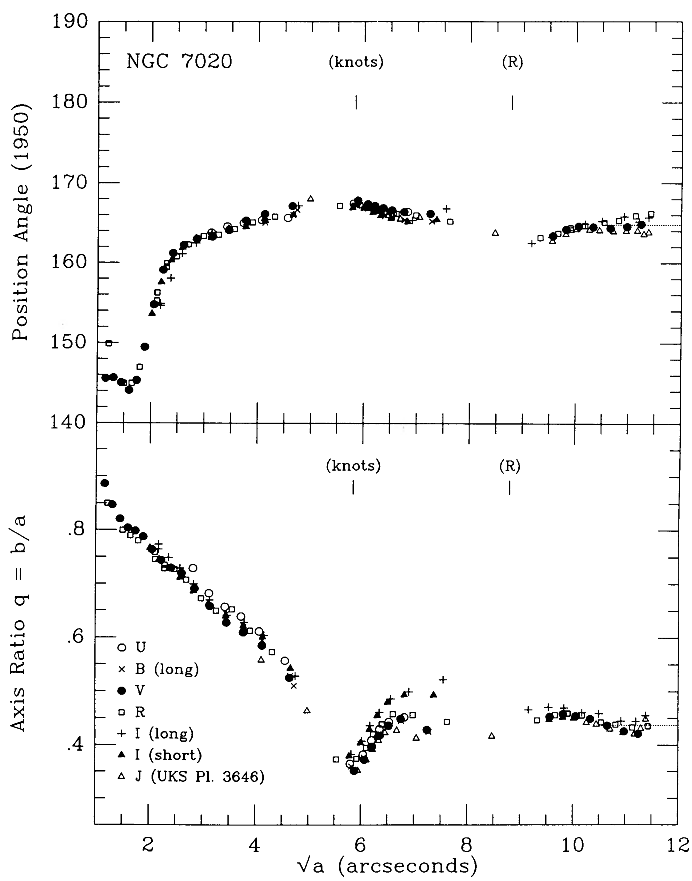


FIG. 6.—Dependence of isophote shapes and orientations (in degrees) on position within NGC 7020, based on ellipse fits.

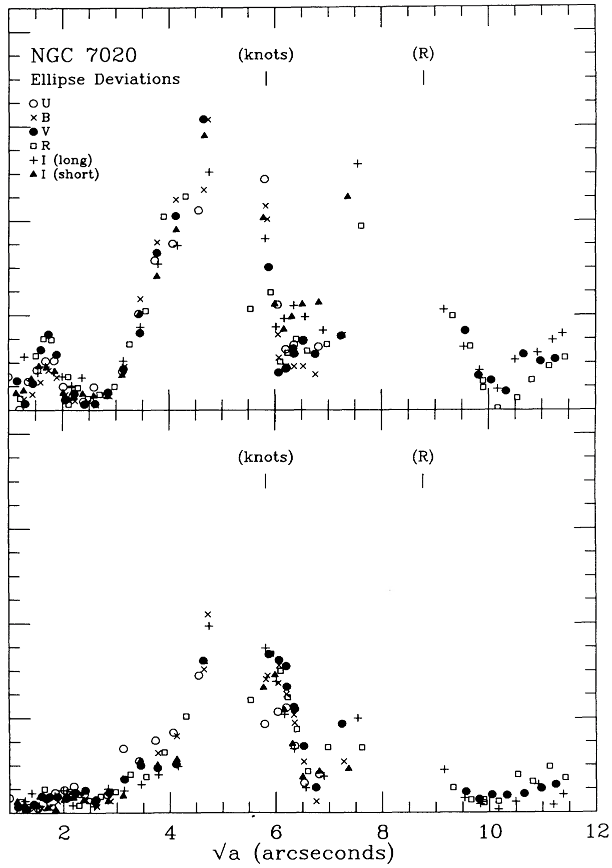


FIG. 7.—Relative amplitudes of the $4\theta$ and $6\theta$ Fourier components of deviations of isophotes from ellipses. Different symbols refer to different filters as indicated. The major-axis positions of the knots and outer ring (R) are indicated.

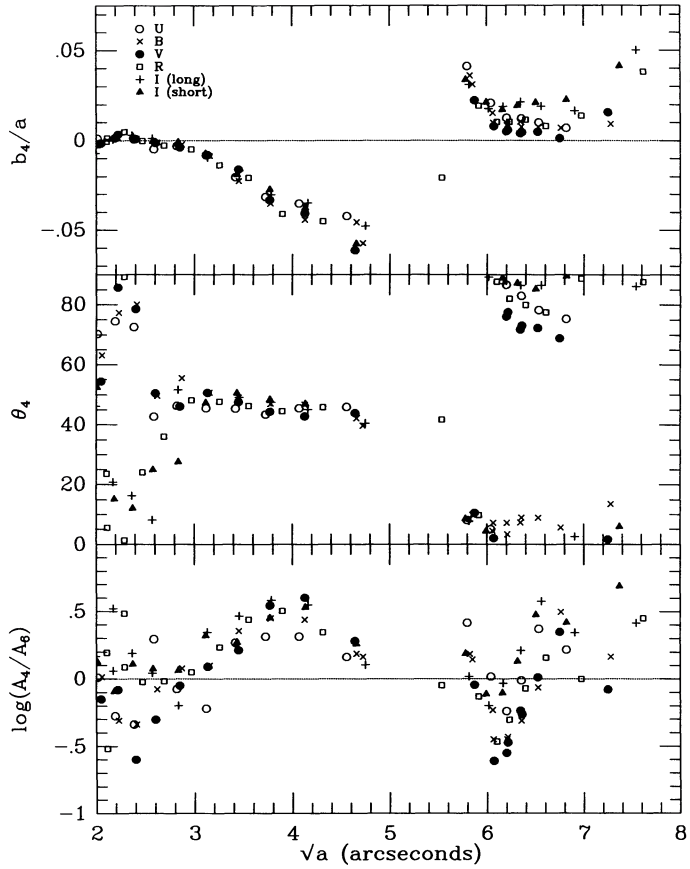


FIG. 8.—Variations with radius of the normalized cos $4\theta$ amplitude, $b_4$; the phase in degrees of the $4\theta$ term, $\theta_4$; and the $m = 4$ and $m = 6$ amplitude ratio, $A_4/A_6$, of deviations of isophotes from ellipses.

therein). If $b_4$ is negative the isophotes are boxy, while if $b_4$ is positive the isophotes are pointed ovals. The top panel of Figure 8 shows that $b_4$ is negative for $9'' \leq a \leq 25''$. This corresponds to the obviously boxy region in Figure 5; the phase $\theta_4$ is very close to 45° over this whole region, as would be expected. In contrast, the sign of $b_4$ is positive for $34'' \leq a \leq 52''$, and the phase $\theta_4$ is near 0° and 90°. This indicates that the isophotes are pointed ovals in this region; one outside the hexagonal zone is visible in Figure 4.

Luminosity and color profiles along the major and minor axes of NGC 7020 are shown in Figure 9. These are based on linear interpolations using full resolution in the inner 10″, $2 \times 2$ pixel binned arrays in intermediate radii, and $4 \times 4$ pixel binned arrays in the outer regions. For $V$, $R$, and $I$ the profiles are based on an average of those from the mosaic images and the central images; along the major axis these cover the greatest radius range. The peaks at $r = 34''$ are not due to an inner ring but indicate the enhancement of surface brightness associated with the bright knots along the major axis. These knots show no real difference in color compared with regions inside or outside their position, as indicated by the color index maps. In blue light the peak knot surface brightness is $\mu_B = 22.27$ mag arcsec$^{-2}$ but the major-axis position angle does not pass exactly through the knots. At the apparent radius corresponding to the same true radius along the minor axis ($r = 15''$), the surface brightness is $\mu_B = 22.9$ mag arcsec$^{-2}$. There is, in fact, little enhancement associated with the hexagonal zone along the minor axis.

The outer ring is visible in Figure 9 mostly as a plateau which peaks near $r = 77''$ along the major axis. It reaches a peak surface brightness of $\mu_V = 23.0$ mag arcsec$^{-2}$ along the major axis and 23.2 mag arcsec$^{-2}$ along the minor axis. In blue light we can directly estimate the outer ring surface brightness along the minor axis from the central $B$-band image, but the major-axis surface brightness must be inferred from the $V$-band image. The corresponding values are $\mu_B = 24.1$ mag arcsec$^{-2}$ (minor axis) and $\mu_B = 23.9$ mag arcsec$^{-2}$ (major axis). The outer ring of NGC 7020 is thus more than 4 times as bright as the outer ring of NGC 3081 along its major axis. The outer ring of NGC 7020 is also everywhere detached from the inner hexagonal zone, while that in NGC 3081 connects to the major-axis points of the inner ring zone and is enhanced at the connections.

Figure 9 also shows that colors along the minor axis involving the $I$ band experience an inverse behavior in the inner regions. As mentioned in § II, this region is suspect (see Fig. 1). The dip in color associated with the outer ring is, however, most probably real and is best represented in the $U-I$ minor-axis profile.

Elliptically averaged profiles of NGC 7020 are compiled in Table 4. These are based on the disk axis ratio and position angle in Table 3, and utilize both the central images and the

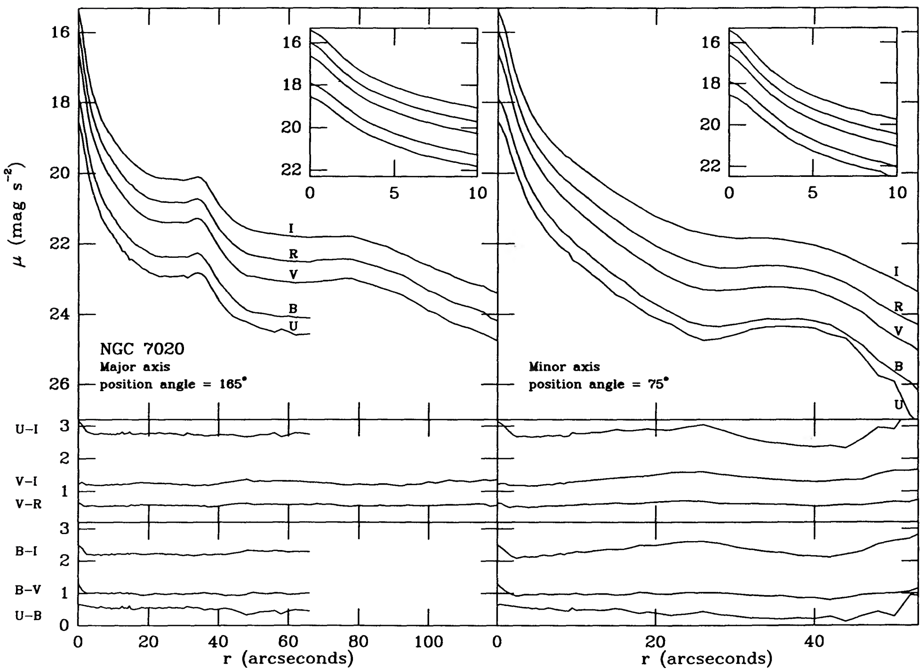


FIG. 9.—Surface brightness and color profiles along the major and minor axes of NGC 7020

TABLE 4

AZIMUTHALLY AVERAGED *UBVRI* PROFILES OF NGC 7020

| r (″) | $\mu_V$ (mag s$^{-2}$) | $B-V$ | $U-B$ | $V-R$ | $V-I$ | r (″) | $\mu_V$ (mag s$^{-2}$) | $B-V$ | $U-B$ | $V-R$ | $V-I$ |
|---|---|---|---|---|---|---|---|---|---|---|---|
| 0.0 | 16.65 | 1.25 | 0.64 | 0.68 | 1.26 | 40.0 | 22.29 | 0.99 | 0.49 | 0.60 | 1.33 |
| 0.5 | 16.82 | 1.19 | 0.66 | 0.67 | 1.26 | 42.0 | 22.47 | 1.00 | 0.49 | 0.61 | 1.36 |
| 1.0 | 17.04 | 1.15 | 0.65 | 0.64 | 1.22 | 44.0 | 22.62 | 1.01 | 0.47 | 0.62 | 1.38 |
| 1.5 | 17.31 | 1.11 | 0.64 | 0.58 | 1.21 | 46.0 | 22.75 | 1.01 | 0.42 | 0.62 | 1.40 |
| 2.0 | 17.59 | 1.06 | 0.63 | 0.57 | 1.16 | 48.0 | 22.86 | 1.00 | 0.44 | 0.63 | 1.41 |
| 3.0 | 18.06 | 1.01 | 0.62 | 0.54 | 1.15 | 50.0 | 22.94 | 0.99 | 0.41 | 0.64 | 1.41 |
| 4.0 | 18.46 | 1.00 | 0.60 | 0.54 | 1.14 | 52.0 | 23.00 | 1.00 | 0.43 | 0.63 | 1.41 |
| 5.0 | 18.79 | 0.99 | 0.58 | 0.54 | 1.14 | 54.0 | 23.06 | 1.01 | 0.43 | 0.64 | 1.41 |
| 6.0 | 19.09 | 0.98 | 0.56 | 0.54 | 1.15 | 56.0 | 23.12 | 1.01 | 0.47 | 0.64 | 1.41 |
| 7.0 | 19.36 | 0.97 | 0.56 | 0.54 | 1.16 | 58.0 | 23.16 | 1.03 | 0.41 | 0.63 | 1.42 |
| 8.0 | 19.58 | 0.97 | 0.56 | 0.54 | 1.17 | 60.0 | 23.19 | 0.96 | 0.42 | 0.63 | 1.41 |
| 9.0 | 19.77 | 0.97 | 0.55 | 0.55 | 1.18 | 62.0 | 23.23 | 0.95 | 0.44 | 0.63 | 1.40 |
| 10.0 | 19.93 | 0.98 | 0.54 | 0.55 | 1.19 | 64.0 | 23.23 | 0.97 | 0.40 | 0.63 | 1.39 |
| 11.0 | 20.09 | 0.97 | 0.53 | 0.56 | 1.20 | 68.0 | 23.24 | .... | .... | 0.64 | 1.37 |
| 12.0 | 20.22 | 0.98 | 0.53 | 0.56 | 1.20 | 72.0 | 23.19 | .... | .... | 0.62 | 1.33 |
| 13.0 | 20.35 | 0.98 | 0.53 | 0.56 | 1.21 | 76.0 | 23.14 | .... | .... | 0.58 | 1.28 |
| 14.0 | 20.46 | 0.98 | 0.53 | 0.56 | 1.22 | 80.0 | 23.15 | .... | .... | 0.57 | 1.26 |
| 15.0 | 20.57 | 0.98 | 0.53 | 0.57 | 1.22 | 84.0 | 23.21 | .... | .... | 0.56 | 1.25 |
| 16.0 | 20.67 | 0.97 | 0.53 | 0.57 | 1.23 | 88.0 | 23.30 | .... | .... | 0.55 | 1.24 |
| 17.0 | 20.77 | 0.98 | 0.53 | 0.57 | 1.24 | 92.0 | 23.43 | .... | .... | 0.56 | 1.24 |
| 18.0 | 20.86 | 0.97 | 0.53 | 0.57 | 1.25 | 96.0 | 23.60 | .... | .... | 0.56 | 1.25 |
| 19.0 | 20.94 | 0.97 | 0.53 | 0.57 | 1.25 | 100.0 | 23.82 | .... | .... | 0.56 | 1.30 |
| 20.0 | 21.01 | 0.98 | 0.54 | 0.58 | 1.25 | 104.0 | 24.03 | .... | .... | 0.57 | 1.32 |
| 22.0 | 21.13 | 0.98 | 0.54 | 0.58 | 1.26 | 108.0 | 24.24 | .... | .... | 0.59 | 1.36 |
| 24.0 | 21.24 | 0.98 | 0.53 | 0.58 | 1.27 | 112.0 | 24.46 | .... | .... | 0.63 | 1.41 |
| 26.0 | 21.33 | 0.99 | 0.53 | 0.59 | 1.27 | 116.0 | 24.66 | .... | .... | 0.66 | 1.45 |
| 28.0 | 21.42 | 0.99 | 0.53 | 0.59 | 1.27 | 120.0 | 24.85 | .... | .... | 0.66 | 1.48 |
| 30.0 | 21.51 | 0.99 | 0.52 | 0.59 | 1.27 | 124.0 | 25.04 | .... | .... | 0.69 | 1.52 |
| 32.0 | 21.60 | 1.00 | 0.52 | 0.58 | 1.27 | 128.0 | 25.23 | .... | .... | 0.74 | 1.57 |
| 34.0 | 21.70 | 1.00 | 0.51 | 0.58 | 1.27 | 132.0 | 25.43 | .... | .... | 0.75 | 1.65 |
| 36.0 | 21.86 | 1.00 | 0.50 | 0.58 | 1.28 | 136.0 | 25.65 | .... | .... | 0.80 | 1.70 |
| 38.0 | 22.07 | 1.00 | 0.47 | 0.58 | 1.30 | 140.0 | 25.91 | .... | .... | 0.83 | 1.75 |

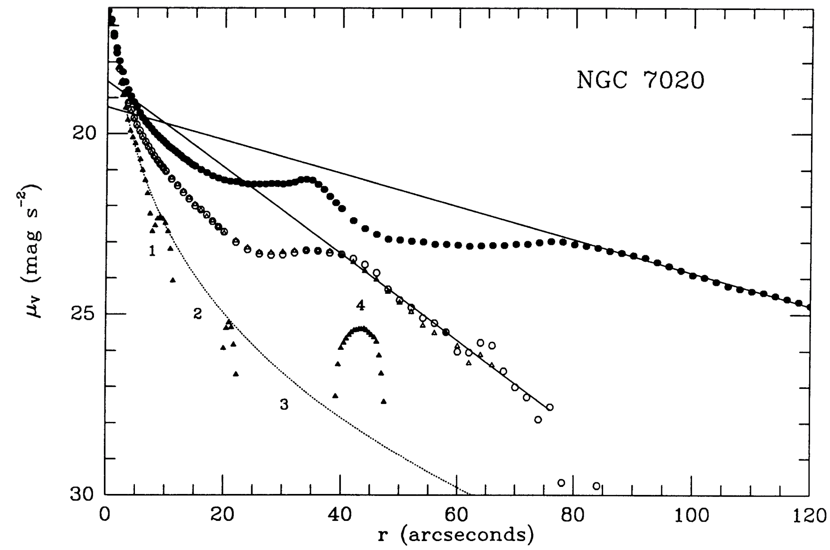


FIG. 10.—Bulge and disk representations for the $V$-band mosaic image. Filled circles refer to the major axis, open circles to the minor axis, open triangles to the minor axis based on the central $V$-band image, and filled triangles to the bulge decomposition based on Kent's (1986) method (see text). Solid lines refer to exponential fits to the outer disk (eqs. [1] and [2]) while the dotted curve is based on eq. (3).

mosaics. Except for the region of the knots, they very much resemble the major-axis profiles in Figure 9 and so are not illustrated separately.

### *d) Profile Decomposition, Deprojected Image, and Fourier Intensity Amplitudes*

Figure 10 shows properties of the bulge and disk components of NGC 7020 based on the $V$-band mosaic image. In this plot, the minor-axis profile is extended beyond those in Figure 9 to illustrate the exponential character of the surface brightness beyond the outer ring; this character extends to 3.1 scale lengths along this axis compared with only about 1.4 scale lengths along the major axis. The relationships derived are as follows:

Major axis ($90'' \leq r \leq 120''$):

$$\mu_V^{\mathrm{II}} = 19.254(\pm 0.116) + 0.046(\pm 0.001)r . \quad (1)$$

Minor axis ($48'' \leq r \leq 76''$):

$$\mu_V^{\mathrm{II}} = 18.526(\pm 0.504) + 0.120(\pm 0.008)r . \quad (2)$$

Here the superscript II follows notation used for the disk component by Simien and de Vaucouleurs (1986). The extrapolated central surface brightnesses differ by 0.73 mag arcsec$^{-2}$ but this is probably not significant considering the low surface brightnesses involved and the small range available for the major-axis fit. The average central surface brightness from the two axes is $\langle V(0) \rangle = 18.9$ mag arcsec$^{-2}$, which corresponds to $B(0)_c \sim 20.6 \pm 0.4$ mag arcsec$^{-2}$ in the notation of Freeman (1970). This value is more than 3 $\sigma$ brighter than the mean, 21.65, obtained by Freeman from 28 spirals.

A reliable bulge model for NGC 7020 could not be obtained from the usual decomposition techniques (e.g., Kormendy 1977; Tsikoudi 1977; Burstein 1979). This is because the obviously bulge-dominated region extends at most to $r = 2\overset{''}{.}5$ (5 pixels) along the minor axis, a range too small to allow a reliable estimate of the slope of a de Vaucouleurs $r^{1/4}$ law; the result would be too sensitive to the adopted seeing corrections. It was found that the best of such fits to the minor axis in $B$ and $V$ predicted a considerable amount of bulge light to be present in the "gap" and beyond the outer ring, regions where the disk clearly dominates. For this reason, I used the more direct technique proposed by Kent (1986), which does not depend on any particular fitting functions. This method combines the information from the major- and minor-axis profiles and requires that the bulge and disk be described by isophotes of different constant flattening, $f$, with $f_d > f_b$. The results of the method as applied to NGC 7020 proved difficult to interpret because the galaxy does not strictly satisfy these requirements. For example, the "knots" strongly affect the major-axis profile, but have no analog along the minor axis. Thus, the following procedure was used. A test of the method was made using simulated profiles based on an $r^{1/4}$ bulge and exponential disk using various input flattenings. In addition, the contributions of features like the "knots" and an outer ring were simulated by adding Gaussian components to the profiles. It was found that in the simplest case where only the bulge and the disk contributed, Kent's method recovered the input bulge model very well. However, adding features such "knots" or an outer ring caused complications, and information on the bulge was lost in certain regions depending on the radii of the simulated features.

These simulations allowed me to make the judgments illustrated in Figure 10, where the results of Kent's method as applied to NGC 7020 are plotted as filled triangles and the dotted curve is the adopted bulge model. To apply the method most effectively, the major and minor-axis profiles from the $V$-band mosaic image were interpolated in $0\overset{''}{.}5$ intervals to radii of 120″; however, to improve signal-to-noise ratio in the outer parts, the surface brightnesses were replaced by equation (1) beyond $r = 90''$ along the major axis and by equation (2) beyond $r = 48''$ along the minor axis. The adopted flattenings ($a/b$) were $f_b = 1.15$ and $f_d = 2.27$. The four labeled zones in Figure 10 are regions where the bulge information has been lost because of structure in the disk. It was found from the simulations that only the upper envelope of points between

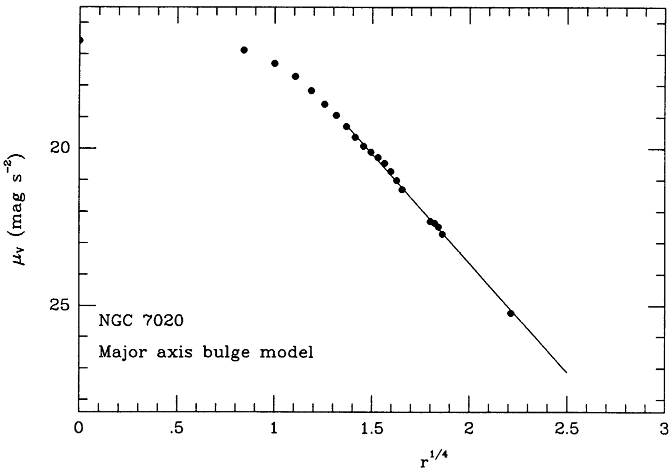


FIG. 11.—Adopted bulge representation in the $V$-band based on Kent's method, versus $r^{1/4}$. The solid line is based on eq. (3).

zones 1 and 3 could be trusted to give information on the bulge. The usable points are plotted in Figure 11 and show an $r^{1/4}$ behavior outside the seeing-dominated region. Restricting to $r \geq 3''.5$, the relation defined by the solid line in Figure 11 is

$$\mu_V^{\rm I} = 9.724(\pm 0.133) + 6.962(\pm 0.087)r^{1/4} , \qquad (3)$$

where $r$ is a major-axis radius and the superscript I follows the notation for the bulge component used by Simien and de Vaucouleurs (1986). Equation (3) is uncertain beyond $r = 10''.5$, but, as shown by the dotted curve in Figure 10, it gives a reasonable result for the bulge contribution at large radii. Equation (3) implies an effective radius $a_e(V) = 2''.0$, an effective surface brightness $\mu_e(V) = 18.05$ mag arcsec$^{-2}$, and a relative bulge contribution (if extrapolated) of $k_{\rm I}(V) = 0.27$. This latter value implies a relative $B$-band contribution of $k_{\rm I}(B) = 0.25$, which would be a smaller than average contribution for an S0$^+$ galaxy (Simien and de Vaucouleurs 1986). The effective surface brightness reduced to the $B$ band would also be near the upper limit for S0 galaxies according to Figure 6$a$ of Simien and de Vaucouleurs (1986).

Figure 12 (Plate 4) shows a deprojected image of NGC 7020 based on the $V$-band mosaic and interpolation of the bulge representation in Figure 11, using equation (3) beyond $r = 3''.5$. The image was obtained by first subtracting this representation from the projected image using a flattening $f_b = 1.15$, and then deprojecting the residual disk surface brightnesses using the disk orientation [$\theta$(d) = 165°] and flattening ($f_d$ = 2.27). The IRAF routine (IMLINTRAN) was used in flux-conserving mode to rotate the image so that the $x$-axis is along the major axis of the galaxy, and then to stretch the image perpendicular to this axis. The bulge was then added back with circular isophotes to the deprojected disk array. Since the more spherical shape of the bulge has been allowed for in the deprojection, that structure is not artifically stretched. However, all parts of the apparent disk are assumed to be infinitesimally thin, which is a limitation that must be kept in mind. The result shows the interesting structure of the hexagonal zone and the near-circular shape of the outer ring. The appearance of the ring is similar to that in Hoag's object displayed in the high-quality images obtained by Schweizer *et al.* (1987). Only the inner zones are dissimilar between the two objects.

Figure 12 also shows that correcting for the shape of the bulge slightly enhances the appearance of the X-shape. The orientations of the arms of the X in projection were measured using a TV display and cursor and the bulge-subtracted image (Fig. 2$b$). Within the uncertainties, the two arms have position angles of $\pm 25°$ with respect to the line passing through the two major-axis knots. In the deprojected image, the angles are about $\pm 47°$. In this same image the ratio of the two longer sides of the hexagon to the mean length of the four shorter sides is about $1.65 \pm 0.15$. These parameters are discussed further in § V.

Finally, the adopted bulge model allows calculation of bulge-corrected relative Fourier intensity amplitudes. These were obtained for $m$ = 1–6 from the bulge-subtracted disk array using the same procedure as described by Buta (1987) for NGC 7531. The final relative amplitudes and phases include the bulge and are illustrated in Figure 13. They are plotted against the radius normalized to that of the $\mu_B = 25.0$ mag arcsec$^{-2}$ isophote, $r_{25} = 103''$. The peak in the relative $m = 2$ amplitudes is caused by the knots, but the amplitudes both inside and outside these features are much smaller; deviations from axisymmetry are, in fact, fairly small over most of the disk of the galaxy. The hexagonal shape of the inner zone is detected just beyond the knots, where the $m = 6$ amplitude actually exceeds the $m = 4$ amplitude. Mildly significant $m = 1$ amplitude is detected over most of the disk beyond the knots, especially at radii $r/r_{25} > 1.2$. This latter region is probably affected by scattered light from the star just outside the field to the north.

### e) *Colors of Features*

The colors of the various features in NGC 7020 are compiled in Table 5. These are means of estimates in small circular apertures placed on a feature; in the case of the outer ring and gap colors, the means are based on 30–40 points placed along the ridgeline as estimated on a TV display. The feature labeled "lens" in Table 5 refers to the mean of two regions located at $r = 23''$ along the line joining the knots; it is meant to represent the underlying component of the hexagonal/X zone. The lens and knots of NGC 7020 are seen to be nearly as red as the bulge (which is assumed to dominate the light inside $r = 3''$). The knots are therefore significant enhancements of old stars. The outer ring is much bluer even than the gap and is clearly a site of recent star formation. If we assume that the color excesses derived from RC2 formulae are applicable to the outer ring alone, then the corrected mean colors of the ring are $(B-V)_0 \approx 0.71$ and $(U-B)_0 \approx 0.14$. These colors lie sufficiently close the galaxy color-color sequence (de Vaucouleurs 1977) to suggest that star formation in the outer ring did not occur in a single burst in the recent past. Rather, the colors are similar to those of a galaxy $10^{10}$ years old having a Salpeter initial mass function (IMF) and a decreasing star formation rate with exponential constant $\beta \approx 4$–5 (Searle, Sargent and Bagnuolo 1973; Larson and Tinsley 1978). This suggests that the outer ring has been a zone of enhanced star formation throughout most of the lifetime of NGC 7020.

## V. DISCUSSION

The observations of NGC 7020 reveal an extremely complex system. As an outer-ringed system, the galaxy is an essentially perfect example, yet the inner hexagonal/X zone sets it apart from most typical ringed galaxies. In this section I discuss two

1990ApJ...356...87B



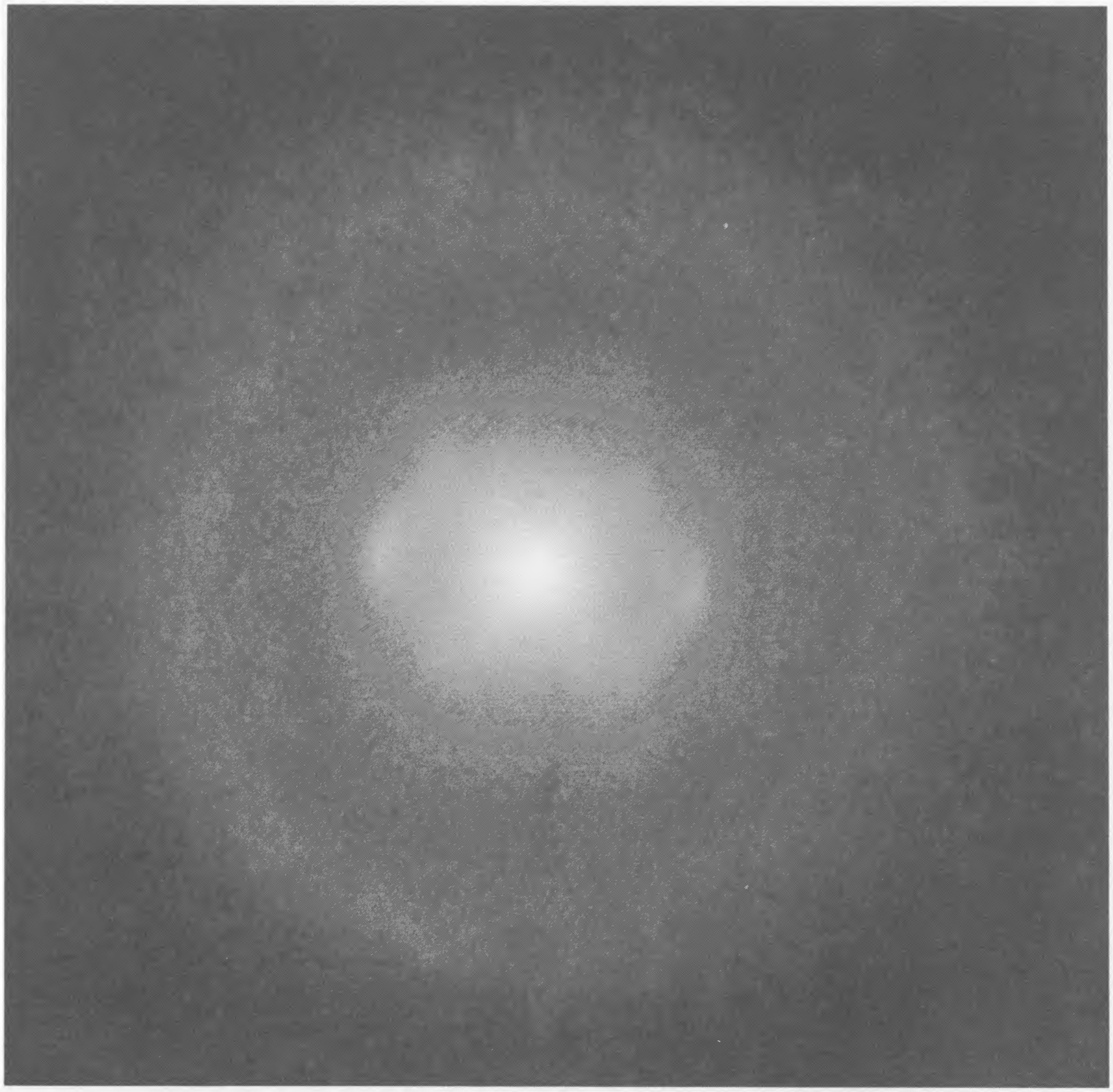

FIG. 12.—Computer-deprojected image of NGC 7020 based on the $V$-band mosaic. The deprojection was performed using a disk axis ratio of 0.44 and a disk position angle of 165°, and allows for the more spherical shape of the bulge using the model illlustrated in Fig. 11 (see text). Dark streak below the nucleus is a defect near the mosaic boundary.

BUTA (*see* **356**, 95)

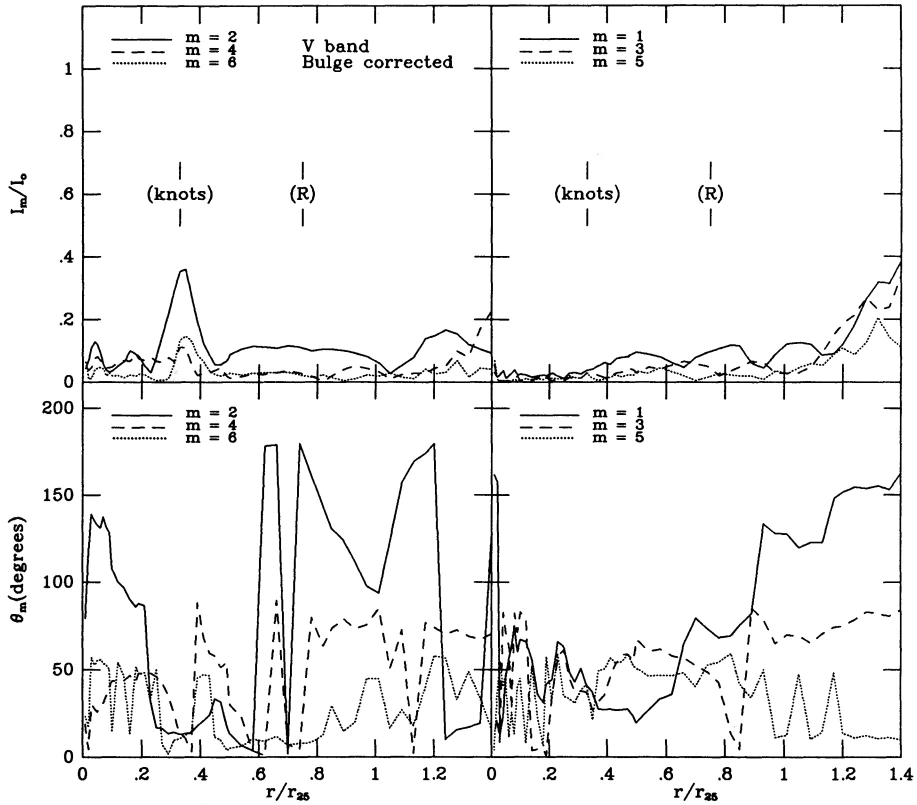


FIG. 13.—Relative Fourier intensity amplitudes for terms $m = 1$–6, based on the bulge-corrected $V$-band mosaic image (see text). The positions of the knots and outer ring (R) are indicated. Phases are measured with respect to the adopted line of nodes.

possible interpretations of the hexagonal/X zone, and then the nature of the outer ring.

### a) *NGC 7020 as an "X-Galaxy"*

The inner region of NGC 7020 displays a bizarre "peanut-shaped" morphology that was striking even when it was seen on the TV display during the initial telescope observations in 1984. It also looks like a figure eight, since the region is enhanced all around, but the basic characterization as an "X" is very clear. Whitmore and Bell (1988) studied another especially good example of this phenomenon, IC 4767, and suggested that the X morphology could be due to accretion of matter associated with a merger or tidal encounter. The idea is that the X morphology is a phenomenon related to polar rings where a small gas-rich satellite galaxy is disrupted into a polar orbit around an S0. If the encounter angle is near 90°, this

TABLE 5

MEAN COLORS OF FEATURES[a]

| Feature | Aperture | ⟨V⟩ (s.d.) | ⟨B−V⟩ (s.d.) | ⟨U−B⟩ (s.d.) | ⟨V−R⟩ (s.d.) | n | Images |
|---|---|---|---|---|---|---|---|
| (R) ............ | 8″ | 18.97 (0.12) | 0.87 (0.08) | 0.25 (0.10) | 0.56 (0.03) | 42 | Centrals |
| (R) ............ | 8 | 18.92 (0.14) | ... | ... | 0.58 (0.03) | 39 | Mosaics |
| Knots .......... | 4 | 18.45 (0.01) | 0.99 (0.01) | 0.55 (0.01) | 0.56 (0.01) | 2 | Centrals |
| Knots .......... | 4 | 18.45 (0.03) | ... | ... | 0.56 (0.01) | 2 | Mosaics |
| Gap ........... | 7 | 19.28 (0.08) | 0.97 (0.05) | 0.39 (0.09) | 0.64 (0.04) | 29 | Centrals |
| Gap ........... | 7 | 19.26 (0.08) | ... | ... | 0.65 (0.06) | 26 | Mosaics |
| Lens[b] .......... | 4 | 18.63 (0.03) | 0.99 (0.01) | 0.55 (0.01) | 0.60 (0.02) | 2 | Centrals |
| Bulge .......... | 6 | 14.24 (0.01) | 1.04 (0.01) | 0.63 (0.01) | 0.57 (0.01) | 2 | Centrals |

[a] s.d. = standard deviation; $n$ = number of regions.
[b] Positioned at $r = \pm 23''$ along position angle 167°.5.

companion is spread into a polar ring, but if the encounter is at a more oblique angle, the companion can settle into the disk through differential precession (Schweizer, Whitmore, and Rubin 1983). However, before merging with the disk, stars can settle into cone-shaped orbits that, when viewed collectively edge-on, appear as an "X." Thus Whitmore and Bell (1988) believe that galaxies like IC 4767 are links between peanut-bulge galaxies and polar rings that imply a common orgin. The possible link is strengthened by the observation that peanut-bulge galaxies tend to lie in cluster or group environments (Jarvis 1986).

Is this a plausible hypothesis for the inner zone of NGC 7020? Several remarks can be made. First, although the inner zone of NGC 7020 resembles IC 4767 to a great extent, it is clearly not being viewed edge-on unless the inner zone and outer ring are not in the same plane or do not have the same flattening. Second, isophotes of the hexagonal zone just beyond the knots are only slightly more elongated than those of the outer ring. When deprojected, this zone stretches into a shape not very different from the outer ring, and appears to be a low-contrast inner ring. Last, NGC 7020 displays remarkable symmetry; apart from the X, there is little evidence for a recent encounter that might link it to Whitmore and Bell's mechanism. These considerations do not rule out the merger/accretion hypothesis, especially since the galaxy does appear to be a member of a group, but they do suggest the following alternative hypothesis.

### *b) NGC 7020 as a Barred Galaxy*

The second hypothesis for the inner zone of NGC 7020 is that it is an unusual ring/lens type of bar or oval distortion. These are features commonly seen in ringed galaxies (see, for example, Buta 1986), and, though not obvious as conventional bars, often they are bounded by subtle ring like enhancements that are quite elongated intrinsically. The typical shape is oval, however, not hexagonal, so the question arises as to what might generate the types of stellar orbits that could give rise to the observed rectangular and hexagonal shapes.

As mentioned in § III, I believe that the non–edge-on orientation of NGC 7020 rules out the possible interpretation that the knots are artifacts of the edge-on view of an inner ring. In S0 galaxies such bright "ansae" are almost always classified as inner rings (for example, de Vaucouleurs 1959, 1963) and it is interesting that they are also observed in IC 4767 (Whitmore and Bell 1988). However, when they are seen in a non–edge-on galaxy, they must be distinct objects. This leads me to consider that NGC 7020 has what might be called a "two-blob" type of bar, that is, a bar which consists of two bright enhancements lined on opposite sides of the bulge. This is actually a fairly common phenomenon and is often seen in ringed galaxies (Buta 1986). A well-known example in a conventional SB0 system is NGC 2859 (Sandage 1961), and others are included in the unpublished Catalogue of Southern Ringed Galaxies (Buta 1986). Occasionally, the blobs are in the form of arches near the major axis of a lens or inner ring. In NGC 7020 the dips in surface brightness between the bulge and the knots, as well as the weak inner ring, do not make the classification as a barred system obvious. If the "two-blob" bar/oval distortion interpretation is correct, then the classification of NGC 7020 should be revised to at least SAB. This has been adopted with uncertainty in Table 3.

If the hexagonal/X zone is an unusual type of bar, how do we interpret its morphology? This has been considered by Contopoulos (1988), who has studied the forms of resonant orbits in an integrable galactic model. He has interpreted the hexagonal zone in NGC 7020 in terms of orbits near the 4:1 resonance (note that in Contopoulos's Fig. 5, NGC 7020 is misidentified as NGC 4321). The orbits of the 4:1 resonance family are box-shaped and elongated along the axis of the bar; he believes these explain the boxy isophotes inside the knots. Near the 4:1 resonance, orbits of the central family (known as $x_1$) are oval and loop at the major axis. Contopoulos believes that these provide an explanation for the knots as well as the six corners of the hexagon, which can be interpreted as a combination of the 4:1 box orbits and the oval $x_1$ orbits. Even the X-shape can be interpreted in terms of loops associated with the corners of some of the 4:1 orbits (see Fig. 4 of Contopoulos 1988). Thus, the structure of the inner zone of NGC 7020 can find a natural explanation in terms of periodic orbits in a bar potential.

There are several difficulties with this bar/resonance interpretation for NGC 7020 that must be noted. The model seems to fit the *projected* appearance of the hexagonal zone better than the deprojected appearance. In projection, the ratio of the length of the longer sides to the mean of the four shorter sides is about 2.6, compared with a predicted ratio in the range 3–5 (see Fig. 2 of Contopoulos 1988; I am grateful to the referee for suggesting that I make this comparison). It was shown in § IV*d* that if the hexagonal zone is as flat as the outer disk, then the deprojected ratio is closer to 1.6, much less than expected. Another difficulty is that the two knots lie very close to the projected major axis, and, as pointed out by the referee, one can only wonder whether this is more than just a coincidence. Finally, also as pointed out by the referee, if the inner zone of NGC 7020 really is a type of bar, why do we not see more examples? These considerations are difficult to evaluate further on the basis of surface photometry alone, but they suggest a few further avenues for research.

One such avenue is the possibility that the inner hexagonal zone of NGC 7020 represents a region which possesses a significant three-dimensional thickness that invalidates the deprojection in Figure 12, at least for that region. Note that three-dimensional *n*-body simulations have developed bars having a box-shaped or even peanut-shaped appearance in the edge-on view (e.g., Combes and Sanders 1981). This character has been interpreted by Pfenniger (1984, 1985) as being due to an important family of 4:1 vertical resonant orbits, but how much this might contribute to the appearance of NGC 7020 is difficult to assess without kinematic observations. Another avenue worth exploring is that the hexagonal shape of the inner zone mostly characterizes an inner ring whose shape is being influenced by 6:1 resonant orbits in the potential of a weak oval distortion. Indeed, de Vaucouleurs (1959; see also de Vaucouleurs and Buta 1980*b*) has emphasized that inner rings in some SAB galaxies have a characteristic hexagonal shape. However, it is uncertain what property of the nonaxisymmetric potential would allow the 6:1 orbits to be sufficiently populated to be so plainly visible in the morphology. Also, sharp corners would be expected mainly for stronger bars and not for weak ones (e.g., Schwarz 1985).

### *c) The Outer Ring*

If we accept the possibility that the inner zone of NGC 7020 is an unusual type of bar, then the outer ring can be naturally explained. The ratio of the diameter of the outer ring to the distance between the knots is 2.3, which is very close to the mean outer to inner ring diameter ratio found in most double-ringed galaxies (Athanassoula *et al.* 1982). This ratio supports the interpretation that the inner hexagonal zone lies near the 4:1 and 6:1 resonances and that the outer ring is linked with the outer Lindblad resonance (under the assumption of a constant-velocity rotation curve). If this is correct, then it is important to explain why the ring is completely detached rather than connected to the inner zone near its major axis, as is typically found. The reason could be that the outer ring of NGC 7020 is associated with the $OLR^+$ family of OLR periodic orbits rather than the usual $OLR^-$ family (Buta 1986). Schwarz (1979, 1981) showed that either of these families can lead to a ring near OLR, but only the family just outside the resonance, that which has an angular momentum slightly greater than circular orbits exactly at OLR, can lead to a completely detached ring well separated from the bar axis and either round or slightly elongated along the bar. Thus the outer ring of NGC 7020 could be a genuine example of an $R_2$ ring, a type found rarely in pure form but usually as a pseudoring (Buta 1986).

On the other hand, if the hexagonal/X zone owes its peculiar morphology to a merger event, then the outer ring could itself be an accretion feature, for example, like that in Hoag's object. This very interesting possibility would mean that the conventional ringed galaxy class does not consist entirely of internally derived structures, which would affect to an unknown extent any interpretations of the statistical properties of rings.

## VI. CONCLUSIONS

The main results of this paper are the following:

1. NGC 7020 is a beautifully symmetric, outer-ringed late S0 or S0/a galaxy. The ring has high contrast compared with those in more typical (R)SB–type galaxies and is completely detached from the inner regions. The "gap" between the ring and the inner zone contains much light.

2. The inner parts of NGC 7020 are very unusual: they show a sequence of distinctive isophote shapes ranging from nearly circular in the inner few arcseconds, to elliptical, to rectangular, to hexagonal, and then to pointed oval. At the ends of the major axis of the hexagonal part there are two bright knots of light which are not likely to be artifacts of an edge-on view of an inner ring.

3. Between the bulge and the knots the light distribution is slightly depressed, and the combination of the rectangular and hexagonal isophotes gives the impression of an "X" in the inner regions. There is no evidence of any very significant color differentiation in this region, the knots, X, and underlying lens being nearly as red as the nucleus. The knots are therefore stellar dynamical phenomena and not associations of young stars. The dips in surface brightness between the knots and the nucleus are not likely to be due to dust.

4. The X morphology is very subtle in projection, but is somewhat more evident in a deprojected image where the shape of the bulge is taken into account. The two arms of the X are found to make angles of $\pm 25°$ in projection with respect to the line joining the two knots, angles which are similar to those observed by Whitmore and Bell (1988) in IC 4767.

5. Although the nature of the inner zone cannot be unambiguously determined from the present observations, I believe that these observations tentatively favor the internal dynamics interpretation, that is, that the inner hexagonal/X zone is related to an unusual type of bar and inner ring. The outer ring and obvious disk make the merger/accretion hypothesis less viable than in a case such as IC 4767, but it is an interpretation which cannot be ruled out completely. If the bar/resonance hypothesis is correct, then we would predict that the inner zone is fairly cold compared with the lenses observed by Kormendy (1984*a*, *b*). This interpretation also suggests that the outer ring could be linked with orbits very close to but *outside* the OLR. Optical spectroscopy and high-resolution H I observations are now needed for a better understanding of this unusual galaxy.

I would like to thank Professor G. Contopoulos for helpful discussions and insights, and D. A. Crocker for helpful comments on the manuscript; and I am very grateful to the referee, E. Athanassoula, for several important suggestions which improved the paper's presentation. I also thank the Royal Observatory, Edinburgh, for providing me with a copy of the SRC *J* plate of the field of NGC 7020.

## REFERENCES

Arp, H. C. 1981, *Ap. J. Suppl.*, **46**, 75.
Athanassoula, E., Bosma, A., Crézé, M., and Schwarz, M. P. 1982, *Astr. Ap.*, **107**, 101.
Bottinelli, L., Gouguenheim, L., Paturel, G., and de Vaucouleurs, G. 1983, *Astr. Ap.*, **118**, 4.
Brosch, N. 1985, *Astr. Ap.*, **153**, 199.
Burstein, D. 1979, *Ap. J.*, **234**, 435.
Buta, R. 1984, Ph.D. thesis, University of Texas.
———. 1986, *Ap. J. Suppl.*, **61**, 609.
———. 1987, *Ap. J. Suppl.*, **64**, 1.
———. 1990*a*, *Ap. J.*, **351**, 62. (Paper I).
———. 1990*b*, *Ap. J.*, in press (Paper II).
Buta, R., and de Vaucouleurs, G. 1983, *Ap. J.*, **266**, 1.
Combes, F., and Sanders, R. H. 1981, *Astr. Ap.*, **96**, 164.
Contopoulos, G. 1988, in *Integrability in Dynamical Systems*, ed. J. R. Buchler, J. R. Ipser, and C. A. Williams (*Ann. NY Acad. Sci.*, Vol. **536**), p. 1.
Corwin, H. G., de Vaucouleurs, A., and de Vaucouleurs, G. 1985, *Southern Galaxy Catalogue* (Univ. Texas Monog., Astr., No. 4) (SGC).
de Vaucouleurs, G. 1948, *Ann. d'Ap.*, **11**, 47.
———. 1953, *M.N.R.A.S.*, **113**, 134.
———. 1956, *Mem. Com. Obs. Mt. Stromlo*, Vol. **3**, No. 13.
———. 1959, *Handbuch der Physik*, Vol. **53**, ed. S. Flügge (Berlin: Springer-Verlag), p. 275.
———. 1963, *Ap. J. Suppl.*, **8**, 31.
———. 1975, *Ap. J. Suppl.*, **29**, 193.
———. 1977, in *The Evolution of Galaxies and Stellar Populations*, ed. B. Tinsley and R. Larson (New Haven: Yale University Observatory), p. 43.
de Vaucouleurs, G., and Buta, R. 1980*a*, *A.J.*, **85**, 637.
de Vaucouleurs, G., and Buta, R. 1980*b*, *Ap. J. Suppl.*, **44**, 451.
de Vaucouleurs, G., and de Vaucouleurs, A. 1964, *Reference Catalogue of Bright Galaxies* (Austin: University of Texas Press).
de Vaucouleurs, G., de Vaucouleurs, A., and Corwin, H. 1976, *Second Reference Catalogue of Bright Galaxies* (Austin: University of Texas Press) (RC2).
de Vaucouleurs, G., de Vaucouleurs, A., Corwin, H., Buta, R.. Paturel, G., and Fouqué, P. 1989, *Third Reference Catalogue of Bright Galaxies*, in preparation (RC3).
Freeman, K. C. 1970, *Ap. J.*, **160**, 811.
Gallagher, J. S., and Wirth, A. 1980, *Ap. J.*, **241**, 567.
Jarvis, B. J. 1986, *A.J.*, **91**, 65.
Jedrzejewski, R. I., Davies, R. L., and Illingworth, G. D. 1987, *A.J.*, **94**, 1508.
Kent, S. M. 1986, *A.J.*, **91**, 1301.
Kormendy, J. 1977, *Ap. J.*, **214**, 359.
———. 1979, *Ap. J.*, **227**, 714.
———. 1982, in *Morphology and Dynamics of Galaxies*, ed. L. Martinet and M. Mayor (Sauverny: Geneva Observatory), p. 113.
———. 1984*a*, *Ap. J.*, **286**, 116.
———. 1984*b*, *Ap. J.*, **286**, 132.
Larson, R. B., and Tinsley, B. M. 1978, *Ap. J.*, **219**, 46.
Lauberts, A. 1982, *The ESO–Uppsala Survey of the ESO (B) Atlas* (Munich: ESO). (ESO *B*).
Lauberts, A., and Sadler, E. M. 1984, *ESO Sci. Rept.*, No. 3.
Lauberts, A., and Valentijn, E. A. 1989, *The Surface Photometry Catalogue of the ESO–Uppsala Galaxies* (Munich: ESO).
Longo, G., and de Vaucouleurs, A. 1983, *A General Catalogue of Photoelectric Magnitudes and Colors in the U, B, V System of 3,578 Galaxies Brighter than the Sixteenth V-Magnitude* (Univ. Texas Monog. Astr., No. 3).

Longo, G., and de Vaucouleurs, A. 1985, *Supplement to the General Catalogue of Photoelectric Magnitudes and Colors in the U, B, V System of Galaxies Brighter than the Sixteenth V-Magnitude* (Univ. Texas Monog. Astr., No. 3A).
Pfenniger, D. 1984, *Astr. Ap.*, **134**, 373.
———. 1985, *Astr. Ap.*, **150**, 112.
Sandage, A. 1961, *The Hubble Atlas of Galaxies* (*Carnegie Inst. Washington Pub.*, No. 618).
Sandage, A., and Tammann, G. A. 1981, *A Revised Shapley-Ames Catalog of Bright Galaxies* (*Carnegie Inst. Washington Pub.*, No. 635) (RSA).
Schwarz, M. P. 1979, Ph.D. thesis, Australian National University.
Schwarz, M. P. 1981, *Ap. J.*, **247**, 77.
———. 1985, *Proc. Astr. Soc. Australia*, **6**, 202.
Schweizer, F., Ford, W. K., Jedrzejewski, R., and Giovanelli, R. 1987, *Ap. J.*, **320**, 454.
Schweizer, F., Whitmore, B. C., and Rubin, V. C. 1983, *AJ.*, **88**, 909.
Searle, L., Sargent, W., and Bagnuolo, W. 1973, *Ap. J.*, **179**, 427.
Shapley, H., and Ames, A. 1932, *Harvard Obs. Ann.*, No. 2.
Simien, F., and de Vaucouleurs, G. 1986, *Ap. J.*, **302**, 564.
Tsikoudi, V. 1977, Ph.D. thesis, University of Texas.
Whitmore, B. C., and Bell, M. 1988, *Ap. J.*, **324**, 741.

RONALD J. BUTA: Department of Physics and Astronomy, University of Alabama, Box 870324, Tuscaloosa, AL 35406